NEUROSCIENCE
INTERNATIONAL BRAIN IBRO RESEARCH ORGANIZATION

RESEARCH ARTICLE

A. G. Zippo et al. / Neuroscience xxx (2018) xxx–xxx

Alternating Dynamics of Segregation and Integration in Human EEG Functional Networks During Working-memory Task

Antonio G. Zippo, [a]* **Pasquale A. Della Rosa,** [b] **Isabella Castiglioni** [a] **and Gabriele E. M. Biella** [a]

[a] *Institute of Molecular Bioimaging and Physiology, Consiglio Nazionale delle Ricerche, Segrate, Milan, Italy*

[b] *Universita' Vita-Salute San Raffaele, Milan, Italy*

Abstract—Brain functional networks show high variability in short time windows but mechanisms governing these transient dynamics remain unknown. In this work, we studied the temporal evolution of functional brain networks involved in a working memory (WM) task while recording high-density electroencephalography (EEG) in human normal subjects. We found that functional brain networks showed an initial phase characterized by an increase of the functional segregation index followed by a second phase where the functional segregation faded after the prevailing the functional integration. Notably, wrong trials were associated with different or disrupted sequences of the segregation-integration profiles and measures of network centrality and modularity were able to identify crucial aspects of the oscillatory network dynamics. Additionally, computational investigations further supported the experimental results. The brain functional organization may respond to the information processing demand of a WM task following a 2-step atomic scheme wherein segregation and integration alternately dominate the functional configurations.

Key words: brain electroencephalographic dynamics, functional connectivity, functional segregation, functional integration, working memory.

INTRODUCTION

The human brain can be portrayed as a giant complex network from the twofold point of view of anatomical and functional perspectives, the former probing the stable structural connections among neurons or neuronal populations, the latter focusing on the functional connections exiting in the huge dynamic repertoire of various transient outputs (actions, perceptions, cognition, etc.) (Tononi et al., 1998; Bullmore and Sporns, 2009, 2012; Park and Friston, 2013). From the functional standpoint, major efforts have been spent to provide quantitative appraisal of brain network dynamic events in different experimental or clinical conditions. Two functional states of brain networks represent a generalized hallmark of brain network dynamics: the functional segregation represented by mutual functional independence of the brain districts, and its counterpart, the functional integration, the ability of the brain to efficiently and contextually combine information from different regions. So far, these principia represent one of the most important paradigms in brain physiology and lay their roots in the realization that brain networks are organized in modules and in few cores of densely interconnected hubs. Modules endorse the ability of brain networks to segregate information while core hubs provide the integration substrate. Many authors also reported brain topological configurations coherent with the small-world network model (Watts and Strogatz, 1998) enriched by a core-periphery organization (van den Heuvel and Sporns, 2011).

So far, most studies on the brain functional connectivity have been carried out on Blood Oxygen Level-Dependent (BOLD) signals in functional magnetic resonance imaging (fMRI). A drawback of fMRI signals is inherent to slowness of the BOLD signal which peaks about 2 s after the neural activity, collapsing the great variability of brain networks highlighted at high temporal resolutions (Whitlow et al., 2011; Chu et al., 2012; Hutchison et al., 2013a). This coarse assumption of stationarity violates most of the brain information processing time-scales which take place over tens or hundreds of milliseconds (Park and Friston, 2013; Sporns, 2013a,b). Despite the brain networks intrinsically and dramatically change over time, the current knowledge about functional networks is primarily achieved under heavy stationarity assumptions.

*Corresponding author.
E-mail address: antonio.zippo@ibfm.cnr.it (A. G. Zippo).

Abbreviations: BA, Barabasi–Albert; BC, betweenness centrality; BOLD, Blood Oxygen Level Dependent; EBC, edge betweenness centrality; EC, eigenvector centralities; EEG, electroencephalography; ER, Erdős–Renyi; fMRI, functional magnetic resonance imaging; RL, ring-lattice; WM, working memory; WPLI, weighted phase lag index; WS, Watts–Strogatz.

https://doi.org/10.1016/j.neuroscience.2017.12.004
0306-4522/

The scope of this work is to study the brain topological information processes within task-evoked events by high-density electroencephalography (EEG) during n-back working memory (WM) tests, which explores short-term memory performance in rapidly changing information environments. In equivalent terms, this means to develop a model for functional brain network non-stationarity during the cognitive task. To this purpose, we recorded the brain activity of 21 healthy volunteers involved in a visual WM task in order to examine the co-activations of large brain regions with 128 channel electroencephalograms. Indeed, previous works suggest that interareal phase synchrony sustains the object representation and the information maintenance in visual WM tasks (Blinowska et al., 2013; Palva et al., 2013).

Our results showed that during the execution of a task, brain networks encountered a first stage dominated by functional segregation followed by a second stage where functional integration prevailed. When participants failed to select the correct answer, we observed different dynamics suggesting that the former pattern was necessary to achieve effective cognitive performances. Further network analyses revealed that the working load of nodes and their core-periphery organization play crucial roles in such dynamics. Further computational *in silico* investigations corroborated the experimental results and provided a formal explanatory theory of the discovered phenomenon.

EXPERIMENTAL PROCEDURES

Ethical statement

The experiment was conducted with the understanding and written consent of each participant according to the Declaration of Helsinki (BMJ 1991; 302: 1194) and in compliance with the APA ethical standards for the treatment of human volunteers (1992, American Psychological Association). The ethics committee of the Carlo Besta Neurological Institute (Milan, Italy) approved the experimental protocol. The whole experiment lasted about one hour and volunteers were not paid for their participation.

Experiment description

We selected 21 young adult subjects (age average = 25, SD = 4; male = 11) and we used a freely available software implementation of the N-back WM task (Jaeggi et al., 2003). Criteria for selection considered anatomical features of the head in order to fit requirements of our EEG cap (GSN-HydroCel-128, EGI). None of the volunteers was taking psychoactive medication and never experienced psychiatric episodes. Subjects were previously instructed about the graphical task interface and a short toy session of the 1-back task was allowed to get a good familiarity with the user interface. Subjects underwent 3 sessions of 41 trials of 1-back task and 3 sessions of 41 trials of 2-back task. The number of trials was a compromise between the highest desirable statistical power and the subject perseverance. The task was constituted by a sequential presentation on a laptop monitor of colored boxes dispersed on a 3×3 matrix (Fig. 1A). Subjects had to keep in mind the color and the position on the screen (out of nine possible). In each trial a colored box appeared on a randomly selected position of the grid for 500 ms. The subjects were asked to respond within 2500 ms by pressing at most 2 buttons to indicate a color or a position match (or both) between the current box and that seen in the previous (one previous for 1-back and two previous for 2-back) trials. Since the used N-back software did not track the timestamps of user responses, we redirected the input system into a Sony Playstation GamePad whose buttons were replaced by touch sensors that simultaneously delivered signals both to the N-back software and to the EGI amplifier.

The subjects were comfortably seated, their arms leaning on a surface to avoid muscle contraction interference and their feet placed on a platform. Participants performed variably on the working-memory tasks averaged and performance was generally good. Indeed, the mean percentage of correct trials was 94.1% ± 6.8 (SD) for 1-back sessions and 89.3% ± 10.6 (SD) for 2-back sessions; the mean reaction time was 0.56 s ± 0.19.

EEG acquisition

We recorded the electroencephalographic activity with a EGI Net Station 400 equipped with a 128 electrode GSN-HydroCel cap. The cap was positioned according to the vendor guidelines by matching three reference electrodes around the scalp (Nasion, i.e. the intersection of the frontal bone and two nasal bones, Inion, i.e. external occipital protuberance and the midpoint between them). Prior to acquisition, we measured amplifier gains and electrode impedances. We fixed those electrodes with impedance values greater than an upper threshold of 70 KOhm by adding few drops of a hydrosaline solution to improve the conductance between the electrode sponge and the scalp. We followed this procedure until all electrode impedances were below the threshold. The wlectroencephalographic signals were acquired at a sampling frequency of 500 Hz. A whole recording session lasted around 30 min.

Since we had no tool to measure the exact position of electrodes or to elucidate the anatomical substrate of participants (e.g. MRI) we excluded any further investigation that involved reliable structural information (cortical mapping, source localization, etc.).

EEG processing

EEG recorded sessions were processed in Matlab with the *eeglab* toolbox (Delorme and Makeig, 2004) and with "in-house" developed routines. Raw signals were mean corrected and filtered (FIR filter, Hamming windowing, 0.1 Hz width, −60 dB of cut-off) in the frequency range [12,45] Hz of interest for beta and low gamma bands. Explorations of related literature and our preliminary analyses (Fig. 1E, F) justified the frequency bands. Specifically, investigations on the WM EEG correlates identified both beta and low gamma as the most influent

Please cite this article in press as: Zippo AG et al. Alternating Dynamics of Segregation and Integration in Human EEG Functional Networks During Working-memory Task. Neuroscience (2017), https://doi.org/10.1016/j.neuroscience.2017.12.004

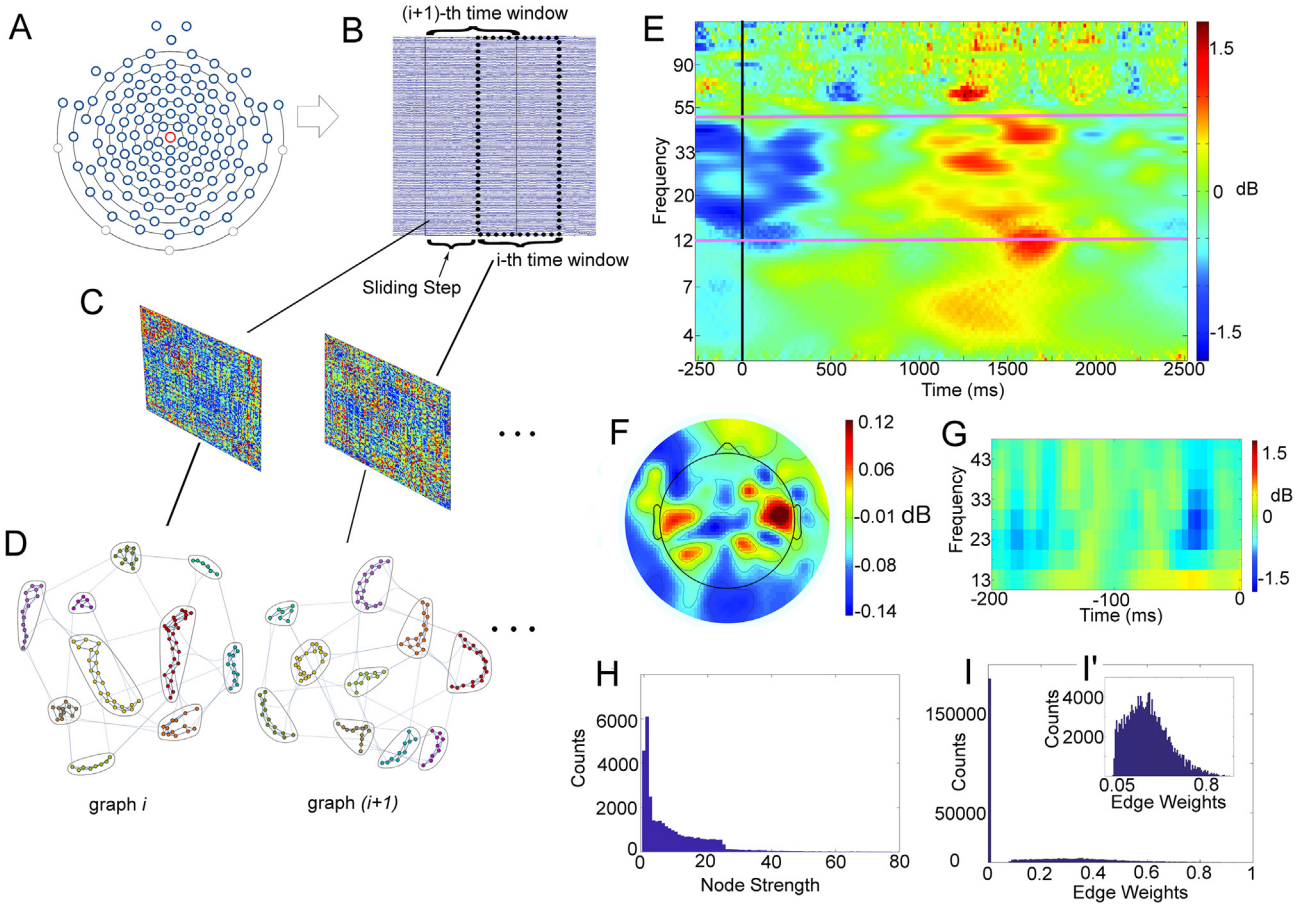

Fig. 1. Design of the experimental framework. (A) Electrode locations in a two-dimensional mapping of human scalp. Locations are referred to the standard positions of the GSN-HydroCel-128 EGI cap in the BESA sphere space. (B) Example of the windowing mechanism used in the study. The ith window is followed by the partially overlapped (i + 1)th window. From the EEG signals from each window a connectivity matrix is extracted (C) by computing the WPLI value for each couple of EEG signals. (D) Graphs obtained from the above adjacency matrices where nodes are displayed according to a community layout. (E) Average Evoked Potentials among all subjects and trials, the most powerful and stable frequency bands elicited by trial trials were the beta and low gamma (12–45 Hz) mainly distributed over the parietal and mediotemporal lobes (F). The average baseline in the interval [−200, 0] ms (G). Distribution of nodal strength (H) and edge weight (I), central values of the latter, explode in the inset (I′).

oscillations. Moreover, another recent work showed that from a functional network perspective, networks extracted from beta and low gamma bands exhibited same basilar properties (Bassett et al., 2009), thus, we decided to combine the extraction of the EEG bands of interest in the range [12,45] Hz to simplify our analyses. Additionally, during the preliminary analysis to investigate the most powerful and stable EEG spectral components elicited by task, signals were filtered to attenuate line noise at 50 Hz using a 0.3-Hz width notch filter (Fig. 1E, F). To remove physiological (eye movement, respiration, heartbeat) and extraphysiological (e.g. instrument, environment) artifacts, we first removed epochs selected by the semi-automated eeglab routine which seeks for abnormal data distributions, spectra and trends under the visual inspection of experts (P.D., G.B.). Then we performed an Independent Component Analysis (ICA) (Delorme and Makeig, 2004) of the signals using the standard algorithm provided in the eeglab toolbox (*runica*). A meticulous visual inspection classified bad independent components opportunely removed from the EEG signals.

Subsequently EEG signals were split into 246 epochs corresponding to the 41 trials of 6n-back sessions. We used a simple sliding window technique which parted the 3 s of interest of each trial in 10 overlapping windows. Specifically, we considered the start of each trial 200 ms before the visual presentation of the box on the screen grid and the end 2800 ms after such event obtaining 10 time windows for each trial. We considered different window sizes variable from 500 ms to 2 s to establish possible conditionings but effects observed in the results kept the statistical significance (data not shown) and we eventually chose a window size of 1 s with a sliding step of 200 ms (timestamps of each window are reported in Table 1). The chosen time window length was short enough to capture great variations of functional connections though preserving robustness of the estimated synchronization index (WPLI).

Functional connection extraction

To extract the functional connections among electrodes in each trial, we evaluated several methods based on synchronization and after a throughout evaluation, we chose the weighted phase lag index (WPLI) because it is capable to minimize effects of volume conduction

Table 1. Time windows in task analysis. All windows had a width of 1000 ms and the sliding step was of 200 ms. Each trial lasted 3 s and for analysis we extracted data samples −200 ms before and 2600 ms after the presentation of the visual pattern

Window number	Left bound (ms)	Right bound (ms)	Centroid (ms)
1	−200	800	300
2	0	1000	500
3	200	1200	700
4	400	1400	900
5	600	1600	1100
6	800	1800	1300
7	1000	2000	1500
8	1200	2200	1700
9	1400	2400	1900
10	1600	2600	2100

which tightly affect high-density EEG recordings (Vinck et al., 2011; Gordon et al., 2013).

Formally, let Z and iZ are respectively the real and imaginary parts of the cross-spectrum of two EEG signals x and y. The Weighted Phase-Lag Index can be defined as:

$$WPLI(x,y) = \frac{|E\{iZ\}|}{E\{|iZ|\}}$$

where E is the expected value and $|\cdot|$ is the absolute value function. The inequality $0 \leqslant WPLI(x,y) \leqslant 1$ holds for each couple of signals x and y and $WPLI(x,y) = 1$ if x and y are maximally synchronized while $WPLI(x,y) = 0$ when there is no synchronization at all. A functional connectivity graph is represented by an adjacency matrix A obtained by computing $A(i,j) = WPLI(i,j)$ for each (i,j) couple of EEG electrodes ($i,j \in \{1,\cdots,128\}$). Eventually, graph edges have been filtered in accordance to the procedure present in a recent work (Dimitriadis et al., 2017). Specifically, 1000 surrogate signals are generated by the Amplitude Adjusted Fourier Transform (AAFT) in order to statistically challenge each graph weight by selecting those that for less than 50 times (out of 1000) were greater in comparison with their correspondent weights computed on the surrogated signal. Additionally, the False Discovery Rate (FDR) criterion furtherly pruned false-positive weights. Because, weighted graphs still remain densely connected a feature hardly matching the structural brain network topology (Rubinov and Sporns, 2011), we used a topological filtering heuristic to prune the connections not fulfilling two of the most important topological principles of brain network: wiring cost optimization and transmission efficiency. We used the already optimized implementation of this algorithm presented in (Dimitriadis et al., 2017).

Network analysis and comparison

Extracted networks were analyzed by the set of complex network statistics reported in Appendix. Functional segregation and integration (Tononi et al., 1994) were estimated respectively by the clustering coefficient (C) and the characteristic path length (L) using the MATLAB implementation provided by the Brain Connectivity Toolbox (BCT) and by other routines developed in our lab (Rubinov and Sporns, 2010).

Some complex network procedures (*small-worldness* and the modularity parameters) required the generation of null networks obtaining either randomization or latticization ensuring however that the node degree distributions of the original graphs were preserved. Randomizations were also weight-distribution conservative as implemented in the Matlab routines *null_model_und_sign.m* and *latmio_und_connected.m*.

The information workflow among node has been furtherly investigated in the extracted functional networks by a couple of network centrality measures: the betweenness and the eigenvector (Borgatti, 2005; Gould, 2016).

We further studied the community structure of our graphs. Instead of using specific modularity algorithms that find coherent node partitions over time slides, we used the Louvain's algorithm to find the best estimation of the modularity index for each time window in each trial in order to evaluate consistent temporal dynamics (*community_louvain.m*). The multi-resolution parameter of Louvain's algorithm (γ), which reduce the well-known tendency of such algorithms to prefer clusters of big size (Lefebvre et al., 2008), has been tweaked for each network by comparison with the randomized version of the same network.

Ultimately, we preferred network analyses on the original weighted version of graphs instead of using binarization techniques for several reasons:

1. unconnected nodes can occur after matrices binarization by thresholding
2. networks varying in size require difficult statistical analyses
3. graph thresholding produces noise reduction but inevitably loss of information
4. the functional connectivity measure (WPLI) has also been proposed to enrich the reduced dynamic range conveyed by its previous version (the PLI) especially for weak interactions (Vinck et al., 2011), the selective removal of weights reduces the WPLI statistical power
5. network thresholding produces a considerable increment of the computational time because different threshold values should be evaluated (see Discussion)
6. all used network statistics have a weighted counterpart (Rubinov and Sporns, 2011)

Computational network models

To investigate the leading factors of the observed topological dynamics we built simulation framework to study the information flow within artificial network models. Thus, we generated two groups of network models, the first containing two network models with brain-like topologies; the second containing two null models. In particular, we produced small-word and core-periphery networks by means of the Watts–Strogatz (WS) and the Barabasi–Albert (BA) models (van den Heuvel et al., 2008). Complementarily, Erdős–Renyi (ER) and the ring-lattice (RL) models represented the completely random and the entirely deterministic

networks. It does not affect the generality of the hypothesis to assume that, for simplicity, synthetic graphs are generated in unweighted form and network statistics used were thus the unweighted versions of those in Appendix.

The information flow within networks was simulated according to the notion of edge betweenness centrality (EBC) which assigns at each edge a centrality score as in betweenness centrality (BC) (Gould, 2016), namely by counting the number of times each edge is involved in the shortest paths between all node couples. For this analysis, we used unweighted simulated networks, namely, the unweighted form of the EBC has been estimated. WS networks were generated with an edge reconnection probability of 0.1.

Although the alternating dynamics observed in the EEG data was constrained in 10 time windows, the core dynamic was deployed and completed in two phases, allowing for dichotomizing the time of flow in two segments within which we expected to observe the alternating dynamics.

From an edge-centric perspective, to simulate the network information flow within the two time halves we computed the rank statistics of the EBC edge distribution which allowed us to part the edges recruited in the first from those in the second phase. Since we could not assume *a priori* the number of activated edges in each phase, we inspected all the possible combinations with the resolution of one percentile. Therefore, we computed and collected both functional graphs for each of the 100 percentiles that served as leverage points along the EBC distribution. Essentially, by keeping a certain set of activated edges in the first phase we labeled and assigned them to the same functional graph in the first-time half. The complementary set of edges not activated in phase 1 fell in the second-time half generating a second functional graph. For both functional graphs, we computed values of functional integration (L) and segregation (C) and 3of the 4 network models were exerted 100 times to evaluate the role of randomness with the obvious exception of the purely deterministic RL model. As a rule, for each generated network we computed the same network statistics (C and L) of the entire graph (all edges together) to track the magnitude of functional evoked modifications because this activated network represented the structural substrate of the evoked functional graphs.

In addition, to elude possible effects of the network dimension, we investigated such dynamics for variable network sizes spanning 6 dyadic scales (2^5 to 2^{10}, where higher scales were prohibitively costly in terms of computational time) and for each network model. The entire computational framework is freely available (https://sites.google.com/site/antoniogiulianozippo/codes), and it is able to reproduce data and figures.

Statistical tests

In this study, different types of statistical hypothesis tests have been adopted. To assess the significance of an estimated Pearson's correlation coefficient between two network statistics, we collated in group #1 the values of all network statistics #1 for all subjects and for group #2 the values of all network statistics #2 for all subjects. Specifically, we used the permutation test by performing 10,000 permutations in each of the two groups, and evaluating the number of times (out of 10,000) the computed correlation was greater than or equal to that computed on the original dataset. Whether the number of times was smaller than 500 (equivalent to get $P < 0.05$, 10,000/500) the null hypothesis was rejected.

When we had to assess if two samples came from different distributions by selecting the non-parametric two-paired Wilcoxon ranksum test. To assess the statistical significance of time-varying network statistics within 10 sliding windows of each trial, the Friedman non-parametric test was chosen and with the Kendall's coefficient of concordance (W) to normalize the Friedman statistics in [0,1]. We preferred non-parametric tests because we had no confidence about the normal distribution of the samples. Eventually, in comparing two distributions the generalized Kolmogorov–Smirnov test has been used. Within the Results section, "*P*" indicates the level of significance and "*N*" indicates the sample dimensions. Statistical quantities are reported by using three decimal digits.

RESULTS

Functional network features

We investigated the dynamics of brain functional networks in simple WM tasks by high-density electroencephalographic recordings in young healthy adults. The WM is responsible for the storage and maintenance enabling integration of higher order information (Oberauer and Suss, 2000; Baddeley and Wilson, 2002; Pessoa et al., 2002; Baddeley, 2003; Oberauer, 2003). WM capacity is expressed through a high level of stability across different cognitive functions, thus relying upon the organization and interaction of multiple brain regions ruled by dynamic changes in cognitive control systems (Jaeggi et al., 2003; Owen et al., 2005).

In this study, we were interested in unraveling short-term dynamics, in terms of brain functional connectivity features, while subjects performed the n-back tasks, and to trace the information flow within WM functional networks. In the n-back task, participants are required to monitor a stream of visual stimuli (colored squared boxes), presented one at a time. The tasks are to indicate whether the currently displayed item is identical as the one presented *n* trials previously. The memory demands grow as *n* increases. In the present study, *n* was set at 1 or 2.

We recorded ten minutes of ongoing (resting) activity before the beginning of the cognitive task and six sequences of 41 trials (i.e. 3 sequences of 1-back and 3 sequences of 2-back). Visual patterns appeared on the screen for 0.5 s at 3 s intervals. In order to study the non-stationarity, we split each recorded trial into 10 sliding time windows, 1 s for each, with sliding steps of 200 ms (see Materials and Methods and Table 1). To extract the functional connections among the 128

electrodes, we used the weighted phase-lag index (WPLI, (Vinck et al., 2011; Ortiz et al., 2012)) thus minimizing the effects of volume conduction that strongly affects EEG recordings. The beta and low gamma frequency bands [12–45] Hz has been selected where we found conspicuous transients of evoked potentials along the temporal, frontal and parietal cortical areas (Fig. 1E, F).

We analyzed the functional connectivity graphs, statistically and topologically supported by complementary analyses, with a set of common network statistics. The extent of functional segregation was estimated by means of two graph-related measures, namely the clustering coefficient (C) and the functional integration through the characteristic path length (L, (Tononi et al., 1998; Rubinov and Sporns, 2010). To investigate the behavior of functional segregation and integration in different experimental conditions we collected network statistics from all recording windows and proceeded with analyses and inferences (Fig. 1A–D reports the analytic approach). The columns of Table 2 summarize the basic network statistics for functional connectivity graphs obtained in 3 different conditions: resting state, 1-back and 2-back tasks. Specifically, we found a tight general correlation between C and L (R = 0.8651, P = 3.451e-12, permutation test, N = 33,600). Subsequently we analyzed C and L in the different experimental conditions and we found that the cognitive task (combining 1- and 2-back, "Overall Trials" in Table 2) produced an increment of C (P = 0.001, N = 33,600, non-parametric Wilcoxon ranksum test) and a decrement of L (P = 0.006, N = 33,600, ranksum test). Furthermore, C values in 1-back trials were smaller than C in 2-back trials (P = 6.9702e-56, N = 33,600, ranksum test) and L values in 1-back trials were greater than in L in 2-back trials (P = 8.630e-37, N = 33,600, ranksum test). These analyses evidenced that the cognitive tasks produced significant changes in the functional network dynamics and that the task difficulty was proportional to the extent of functional segregation and integration.

Dynamics of functional segregation and integration

We proceeded investigating the dynamics of functional segregation and integration within the time windows. By averaging the functional graph statistics on all trials for each subject (see Fig. 2A–F), we found a specific trend within each n-back trial. In particular, between 300 and 700 ms (time windows 2, 3, 4) after the presentation of the visual pattern, the C value (measure of functional segregation) reached its peak then decreasing between 1300 and 1700 ms (time windows 6, 7, 8). Conversely in this same period L reached its minimum (indicating, being an inverse measure of integration, namely a peak of functional integration). Statistical tests (Friedman) showed that C and L variations were significant both considering all trials (C: P = 9.533e-5, L: P = 6.080e-13, N = 51,660) and separately, the 1-back trials (C: P = 1.999e-34, L: P = 2.685e-31, N = 25,830) and the 2-back trials (C: P = 3.101e-40, L: P = 4.319e-90, N = 25,830). Times of maxima and minima were slightly variable among subjects. Again, in all trials C and L were tightly correlated (R = 0.895, P = 0.006, permutation test). Taking into account the C and L minima and maxima in 1-back and 2-back conditions, we found that C maxima were larger (P = 2.417e-26, N = 5166, ranksum test) and C minima were smaller (P = 0.001, N = 5166, ranksum test) in 2-back than in 1-back trials. Complementarily, L maxima were larger (P = 1.602e-44, N = 5166, ranksum test) and L minima were larger (P = 0.007, N = 5166, ranksum test) in 1-back trials. Equivalently, widths of C maximal oscillations were greater in 2-back than in 1-back while widths of L maximal oscillations were greater in 1-back.

To rule out an influenced by functional connectivity modulations, we further analyzed the dynamics of the WPLI synchronization index during the task execution exploring potential correlations with the network statistics above. We noted no significant variations of the average synchronization index along time windows (P = 0.810, N = 33,600, W = 0.853, Friedman test). Consequently, C and L values were not correlated to the average WPLI values (C: R = 0.096, P = 0.002, L: R = 0.084, P = 0.001, permutation tests, N = 33,600).

Altogether these results indicate that the architecture of functional connectivity graphs switched between two specific states, more segregated in the first phase supervened by integration in the second. Secondarily, the results show that greater cognitive loads, as in 2-back compared with 1-back, made networks more integrated and more segregated. Finally, the observed effects were not due to modulations of the WPLI synchronization index.

Occasionally, though the percentage of correctly completed trials was high (∼92% on average), participants got wrong answers to trials. In these cases, the C average distribution strongly differed from that obtained in the correct trials (P = 6.154e-4, N = 10, Kolmogorov–Smirnov test), where the C variations within the task were not significant (P = 0.785, N = 5682, W = 0.643, Friedman test). Similarly, the L average distribution was different (P = 3.894, N = 10, Kolmogorov–Smirnov test) and L variations were not significant (P = 0.720, N = 5682, W = 0.613, Friedman test). Results are shown in Fig. 2G, H. By analyzing the

Table 2. Functional brain network general statistics (mean value, standard deviation). All networks had 128 nodes

Functional network	Average node strength	Average edge weight	Clustering coefficient (C)	Characteristic path length (L)	Small-worldness (S)	Small-worldness (ω)
Resting State	61.468,11.212	0.480,0.271	0.394,0.069	0.081,0.021	2.12,0.56	0.09,0.05
Overall Trials	63.511,11.88	0.492,0.288	0.398,0.116	0.062,0.013	2.34,0.78	0.07,0.03
1-back	64.446,12.201	0.483,0.273	0.389,0.094	0.069,0.019	2.29,0.76	0.06,0.02
2-back	62.577,11.485	0.477,0.285	0.411,0.076	0.057,0.010	2.40,0.81	0.07,0.03

Please cite this article in press as: Zippo AG et al. Alternating Dynamics of Segregation and Integration in Human EEG Functional Networks During Working-memory Task. Neuroscience (2017), https://doi.org/10.1016/j.neuroscience.2017.12.004

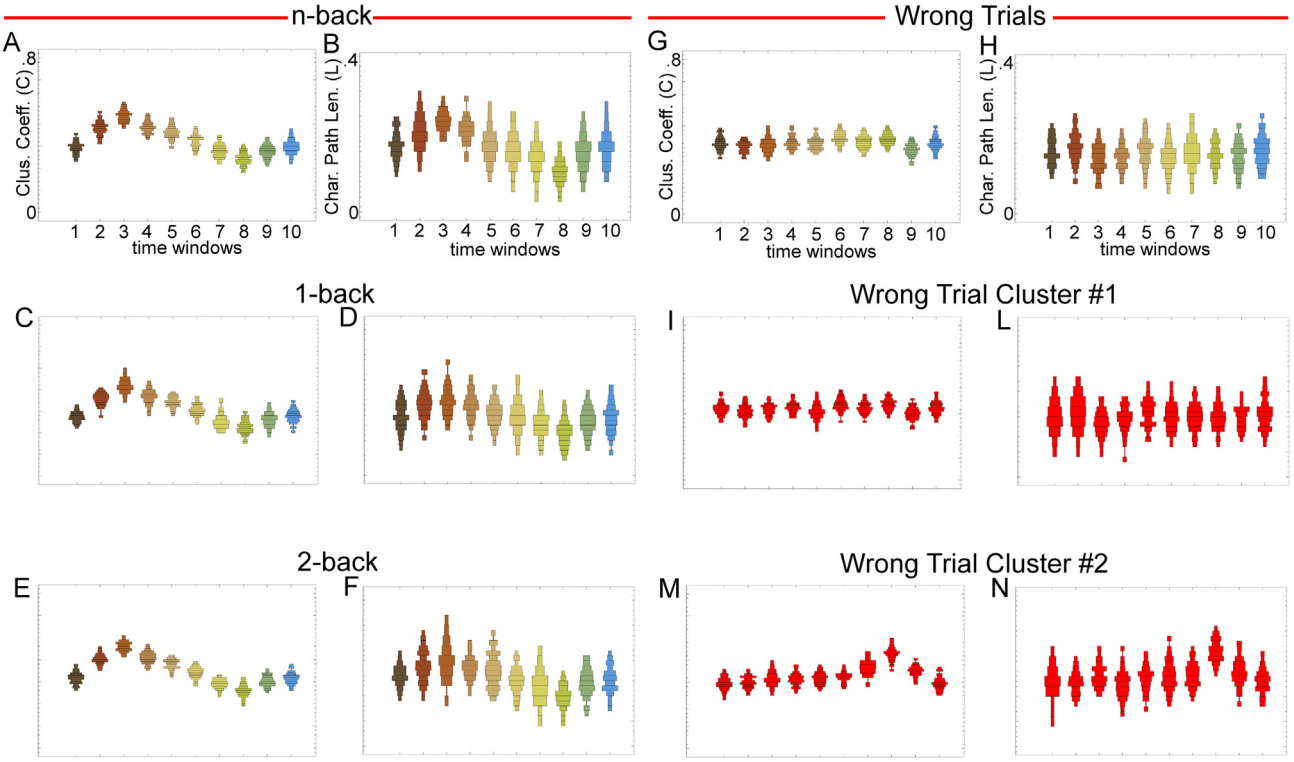

Fig. 2. Dynamics of network statistics during the cognitive task. Plots are obtained averaging all cognitive task trials and all participants. (A, B) Figures clearly indicate a first phase spanning time windows from 2 to 4 (and from 6 to 8) where C and L values reached the maximum (minimum). The figures in (C, D) represent same statistics computed by considering only 1-back trials and in (E, F) only 2-back trials. (G, H) Trends obtained averaging all error trials in all participants. Data analyses revealed two clusters for C and L trends. (I–L) Cluster n.1 where the clustering coefficient variations were not statistical significant within the wrong trials as well as the characteristic path length. In the second cluster (M, N) instead showed a significant modulation of the network statistics within the trials but the C and L maxima were got around the seventh time window. All plots are generated by the ''DistributionChart'' function of Wolfram Mathematica ©.

C and L behaviors in error trials, we isolated two common trends depicted in Fig. 2I-N. In the first kind of trend (Fig. 2I–L) no modulation of C or L appeared while in the second one (Fig. 2M, N) a significant modulation occurred only in the time windows 6–9. These results indicate that, when participants got wrong answers, the corresponding functional connectivity networks did not correctly modulate integration and segregation during those trials. Notably, in the presence of delayed modulations (increments of C or L), there were associated wrong trials. Essentially, we deduced that the first 4–5 time windows correspond to the convenient interval where the first stage of network modifications (increases of functional segregation or decreases of functional integration) must to occur under penalty of a wrong trial.

Network centrality and modularity during WM trials

In a second stage, we aimed to characterize functional connectivity graphs with more complex network statistics (centrality and modularity) able to highlight the information flow dynamics within networks. Typically, this requires measures that estimate the importance of nodes in the network information routing usually addressed by specialized network measures (centrality) of two types: those that use only information of neighbors (local centrality) and those that instead use information from the entire network (global centrality).

Among the local centrality measures we preferred the node degree centrality, a quantitative measure of the number of node connections, whereas, for the measures of global centrality, we chose the betweenness (BC) and the eigenvector centralities (EC) (Borgatti, 2005; Gould, 2016). The former measures the number of times a node is bridging neighboring or far nodes. The latter assigns a greater centrality to a preeminent node (a richly connected node) than to a poorly connected one. We found that the average node degree was correlated with both C (R = 0.629, P = 2.211e-54, N = 51,660, permutation test) and L (R = 0.538, P = 8.404e-30, N = 51,660, permutation test), and that it was modulated during task trials (P = 0.001, N = 51,660, Friedman test). Conversely, the centrality measures appeared to be invariant during task trials (BC: P = 0.999, W = 0.913, EC: P = 0.981, W = 0.912, N = 51,660, Friedman tests, Fig. 3A, B). This last result induced us to further investigate the role of centrality in such brain functional networks by analyzing the distribution of the centrality measures irrespective of the trial time windows. We found that BC and EC showed heavy-tailed distributions (Fig. 3C). The degree centrality on the contrary appeared normally distributed with a slight positive skewness (0.12). These results suggested that

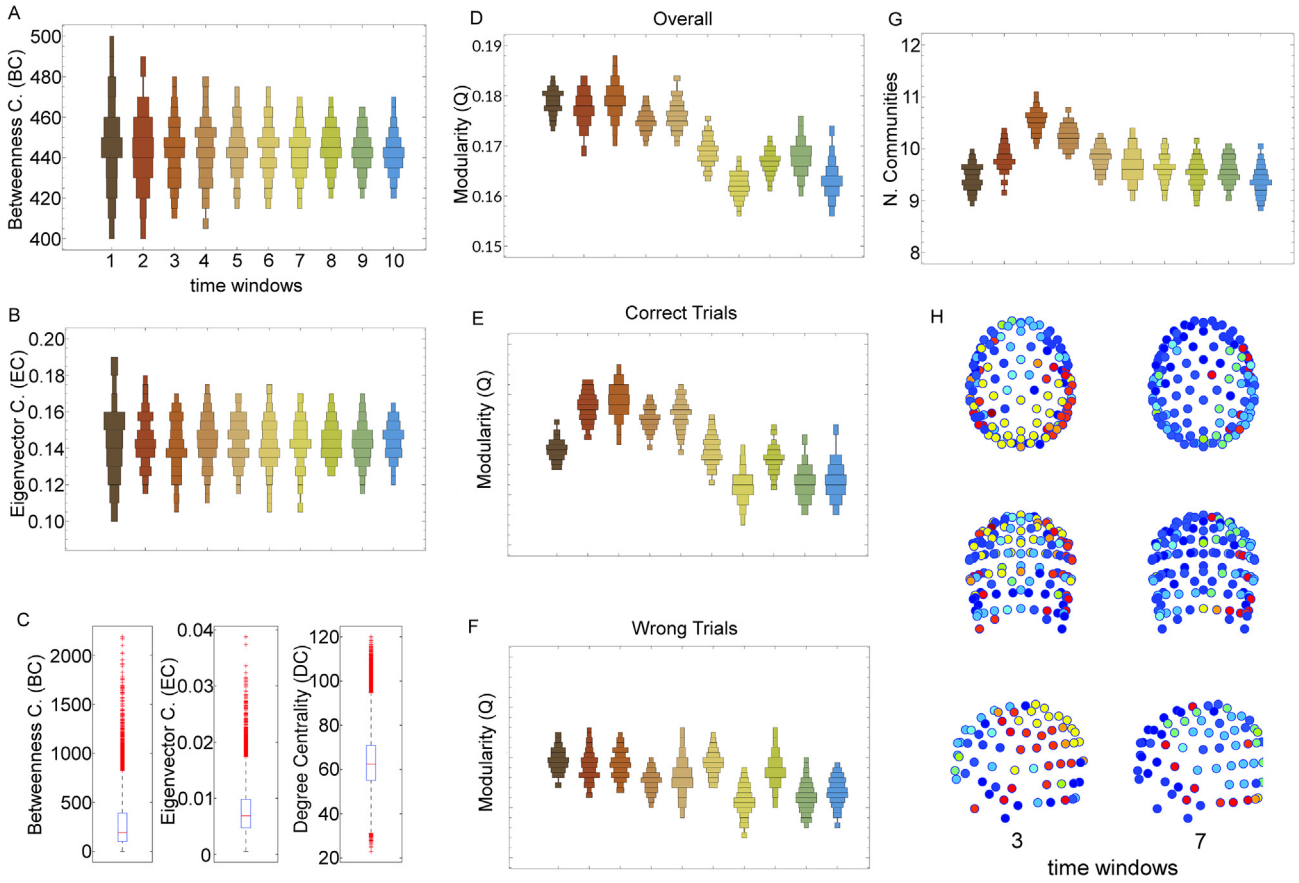

Fig. 3. Centrality and Modularity in brain functional networks. Trends of betweenness (A) and of eigenvector (B) centralities obtained averaging all cognitive task trials and all participants. (C) Distributions of betweenness and eigenvector centralities have heavy-tailed distributions while degree centrality has a Gaussian-like shape. (D) Estimated modularity index, computed considering all trials, where is visible a straightforward dynamical effect not, however, statistical significant. (E) The modularity obtained considering only trials in which participants did correct answers, gave significant effects, with peaks of Q in time windows 2–4 and minima of Q in windows 6–8. For this reason, Q was tightly correlated with C and L. (F) Wrong trials showed no significant modulations of the modularity index. (G) The modification of the number of communities within task trials was significant: when in functional networks prevailed on the functional segregation (Fig. 2), the number of communities increased of 20–30%. (H) Example of community dynamics where the left column plots represent network configurations in the time window 3 and right column plots of time window 7 of a representative trial. Plots in A-B and D-G are generated by the "DistributionChart" function of Wolfram Mathematica ©.

node loads were inhomogeneously distributed among nodes identifying groups of nodes that likely process a much higher amount of information than other ones. In conclusion, global centrality appears to be an important indicator of the node role during the n-back cognitive task because it identifies a stable node configuration during task completion.

Since, other important aspects of complex network dynamics can be hidden in the brain modularity structure, we subsequently performed a network modularity analysis. As a rule, nodes of networks can be clustered into groups (communities or modules) in order to maximize the number of edges within each community and to minimize the number of intercommunity edges (Freeman, 1977). The modularity index Q represents the goodness of the proposed partition and takes values within [0,1]. The modularity was correlated (R = 0.838, P = 2.231e-98, N = 55,166, permutation test) with the clustering coefficient indicating that the modularity increased during peaks of functional segregation and, vice versa, it declined during peaks of functional integration (R = 0.889, P = 0.008, N = 55,166, permutation test). Furthermore, we found that the modularity did not significantly changed during the task trials (P = 0.410, N = 51,660, W = 0.422, Friedman test, Fig. 3D) but when correct trials were extracted, modularity modulations became significant (P = 0.018, N = 47,683, W = 0.130, Friedman test, Fig. 3E). Differently, this did not happen in wrong trials (P = 0.917, N = 3977, W = 0.971, Friedman test, Fig. 3F). Communities represent also a coarse-grain measure of the network information segregation, coupled to the clustering coefficient. Thus, by analyzing the number of communities in task trials, we found that the number of communities was significantly modulated (P = 0.007, N = 51,660, W = 0.133, Friedman test, Fig. 3G) showing a positive slope (∼+20%) in the time windows 2, 3 and 4. This fact suggested that when networks were in functional segregation modality, they had more modules whereas functional integration did not require specific adjustments of the community cardinalities.

In Fig. 3H, network node colors express the membership to community and in the first column (left) appear the communities in the time window 3 and in the

second column (right) the communities of time window 7. Figures highlight that in earliest network configurations dominated by functional segregation preeminence, there are more communities than in the later ones where functional integration prevails. Therefore, modularity changed observing a comparable scheme to that found with a finer-grain measure of segregation (C).

Computational inspections

In the last stage, we tried to figure out the possible factors which enliven the alternating behavior of segregation and integration, the working hypothesis of this section. Therefore, we conjectured that some of the information processing in human brain networks could be mirrored in the observed alternating dynamics.

Hence, we developed a computational model which simulated the information flow within brain networks in comparable conditions, in order to replicate the topological dynamics observed in experimental data. Connectomics studies described the human brain as a small-world network with a strong core-periphery and scale-free organization (Newman, 2006). The core-periphery feature identifies bipartite networks with a partition characterized by densely interconnected nodes with high centrality, and a complementary partition with sparsely interconnected and (usually) non-central nodes. Accordingly to these facts, since functional brain networks have both a small-world and a core-periphery organization (see Table 2 and Results sections), we challenged the working hypothesis against 4 network models: two of them coherent with brain network topologies, namely the Watts–Strogatz model (WS), able to generate small-world networks and the Barabasi–Albert model (BA), able to generate (scale-free) core-periphery networks(van den Heuvel et al., 2008), while on the other hand, 2 null networks, the Erdős–Renyi (ER) and the ring-lattice (RL) models, respectively a network where edges are completely randomly assigned and, conversely, a network with a purely deterministic allocation of edges.

Since the analysis of edge activations is easier from a functional perspective, network dynamics were conveniently analyzed from an edge-centric rather than a node-centric perspective following an approach similar to works of Grady et al. (Senden et al., 2014) and Ekman et al. (Ekman et al., 2012; Grady et al., 2012). Therefore, we directly focused on the aroused functional connections by analyzing a wide range of different activation levels. Essentially, rather than recruiting node-consequent edges, we directly collected edge activities by specific criteria. Namely, we divided the temporal horizon of the events in two succeeding functional phases contriving a condition for the elicitation of the edges. At first, each model network was exerted 100 times to reduce the random effects. In the first trial, the algorithm parted edges such that where EBC was smaller or equal to its first distribution percentile it belonged to the first group, the rest of edges to the second group. Similarly, in the second step the algorithm classified by leveraging at the second percentile and so forth until the last percentile. We investigated such dynamics for a variable size spanning 6 dyadic scales (2^5 to 2^{10}) and for each network model (higher scales were prohibitively costly in terms of computational time). Therefore, for each generated network we computed the network statistics (C and L) to track the evolution of the functional evoked network modifications.

Results from simulations were subsequently filtered to discard singularity cases where C or L were equal to 0 and to select the regions, in terms of network size and leverage range, where the hypothesis was satisfied. We called such regions as *admissible* meaning that if such a network elicited first a certain percentage (leverage point) of edges (functional graph of stage 1) then it would have also elicited the rest of the edges (functional graph of stage 2), we verified our hypothesis (Fig. 4).

We found that the WS and BA models produced relevant sets of admissible regions (see Fig. 5A′–D′), namely intervals of the edge leverage that verified the working hypothesis. Such regions rose with the network size in case of WS networks and shifted towards higher leverage points for BA networks. Importantly also ER

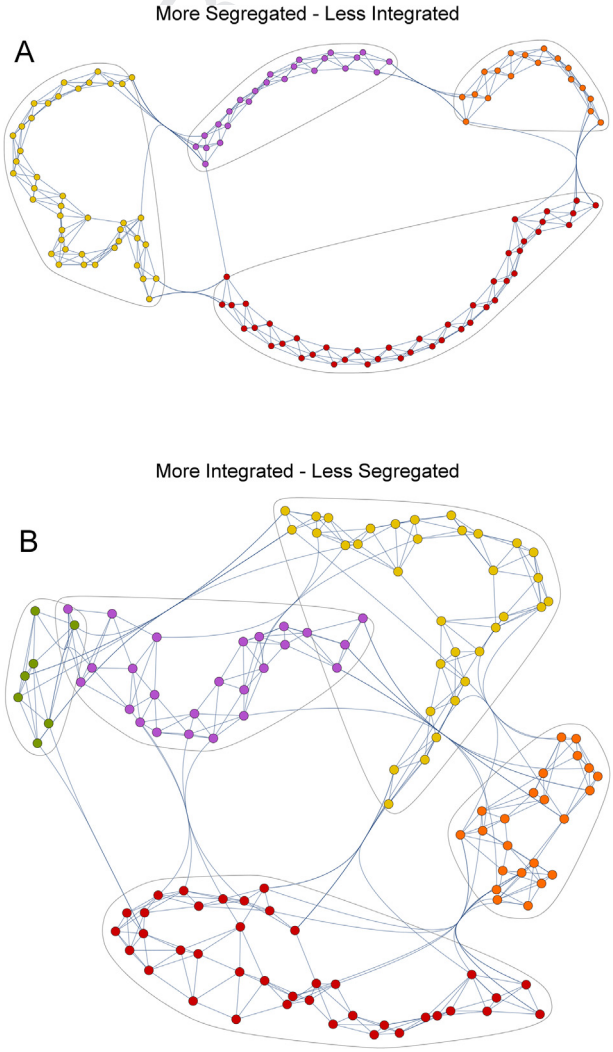

Fig. 4. Example of the biphasic network dynamics. (A) Hypothesized "Phase 1" characterized by a functional segregation prevalence. (B) Hypothesized "Phase 2" characterized by a functional integration dominance. Both configurations were generated by the simulator that used small-world networks with 64 nodes.

models reported a considerable range of admissible regions indicating that purely random networks can be in accordance with the experimental results. In contrast, RL networks generated a quasi-empty set of admissible regions and did not support the proposed hypothesis.

Specifically, in the WS model, when network size grew (greater or equal to 128 nodes) edge leverages nearby or greater to 10% satisfied the working hypothesis. The BA model instead was compatible with leverages in the range from ∼40% to 60–65% for network of size greater or equal to 64 nodes except for the case with 1024 node wherein the admissible leverages were those from 70% or higher. The ER model was compatible in a double interval of admissible regions that were [∼20%, ∼40%] and [∼60%, ∼80%] (for network of sizes 32, 64, 128, 256), the second interval shifting to higher values according to the increasing network size. Networks of size 512 or 1024 had a single admissible region that was [40–50%, 100%]. At last, the RL model was only compatible with a very narrow range of regions and for few network sizes.

By considering the functional changes provoked by the imposed dynamics in comparison to the structural substrate, we noted that in the WS, BA and ER models the Phase 1 and Phase 2 networks largely differed from the original network (green points and excluding C and L values equal to 0), a phenomenon not observed in the RL model. A more representative example where the phenomenon is easily appreciable can be found in the movie Movie 1 built with the C dynamics of a synthetic SWN with 128 nodes.

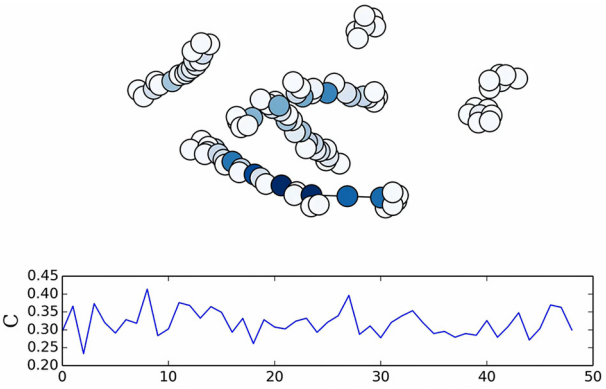

Movie 1. The movie shows a network flow, in terms of functional connection graphs, simulated by a small-world network with 128 nodes tracking the evolution of the clustering coefficient (C). Remarkably, it is evident the oscillation behavior of C that because it was tightly correlated with L visually demonstrate that such networks underwent to two topologically and orthogonal phase likely supporting the information processing demand.

The evidence collected at this stage suggests a stable computational scheme for the information processing within the functional brain organization where each computation might be decomposed in sequences of two atomic and alternating steps (segregation and integration).

DISCUSSION

In this work we investigated by EEG in healthy volunteers the global brain connectivity events during a working-memory task. We found that the temporal evolution of the involved brain network architecture follows steadily a general simple 2-step scheme wherein a surge of functional segregation flows into integration throughout the elaboration of a working-memory task. This mechanism could represent an elementary paradigm orchestrating the brain information processing in small-world networks and, hence, in effectual brain functional dynamics. To confirm this, error trials diverged from this rule.

Previous works

In these last years the study of temporal networks, namely functional networks changing their architectures in time, has progressively encompassed a widening range of disciplines. Temporal networks play an obvious critical role in the studies on brain network dynamics (Lefebvre et al., 2008; Chu et al., 2012; Hutchison et al., 2013b; Sporns, 2013a; Allen et al., 2014). Important papers have forerun crucial issues on brain circuits interpreted as temporal networks. Namely, Betzel et al. studied the repertoire of distinct states encountered by brain functional networks in EEG resting activity observing a limited set of strongly recurrent network states (Betzel et al., 2012) resembling the EEG microstates (fast and transient electrical configurations on the scalp) described elsewhere (Van de Ville et al., 2010). In accordance with these results, we propose here a dynamic network model capturing the early stages of a cognitive task in two connectivity states with inherent recurrences. In accordance with our results, it has been recently reported that during different types of tasks, networks showed higher degrees of integration (Crossley et al., 2013). In contrast, Kitzbichler and colleagues recently reported that global and local efficiencies of functional brain networks showed stable patterns during n-back tasks (Kitzbichler et al., 2011) and this mismatch might be ascribed to problems inherent to distortions induced by volume conductions, potentially injecting masking effects over putative neural sources.

Brain network physiology

Besides these dynamic variables, our results indicate also that a hierarchical information processing could be nested into the alternating segregation and integration couples observed in trials of a working-memory task. Namely, the differences observed between 1-back and 2-back trials in terms of segregation (C) may be ascribed to the fact that a 1-back trial recruits mainly attentional processes in order to confront two successive trials, while a 2-back trial entails both attentional and control processes. The former would emerge in order to process the stream of stimuli, the latter to monitor intervening items and inhibit competing responses allowing the successive integration of the information for correct response selection.

Please cite this article in press as: Zippo AG et al. Alternating Dynamics of Segregation and Integration in Human EEG Functional Networks During Working-memory Task. Neuroscience (2017), https://doi.org/10.1016/j.neuroscience.2017.12.004

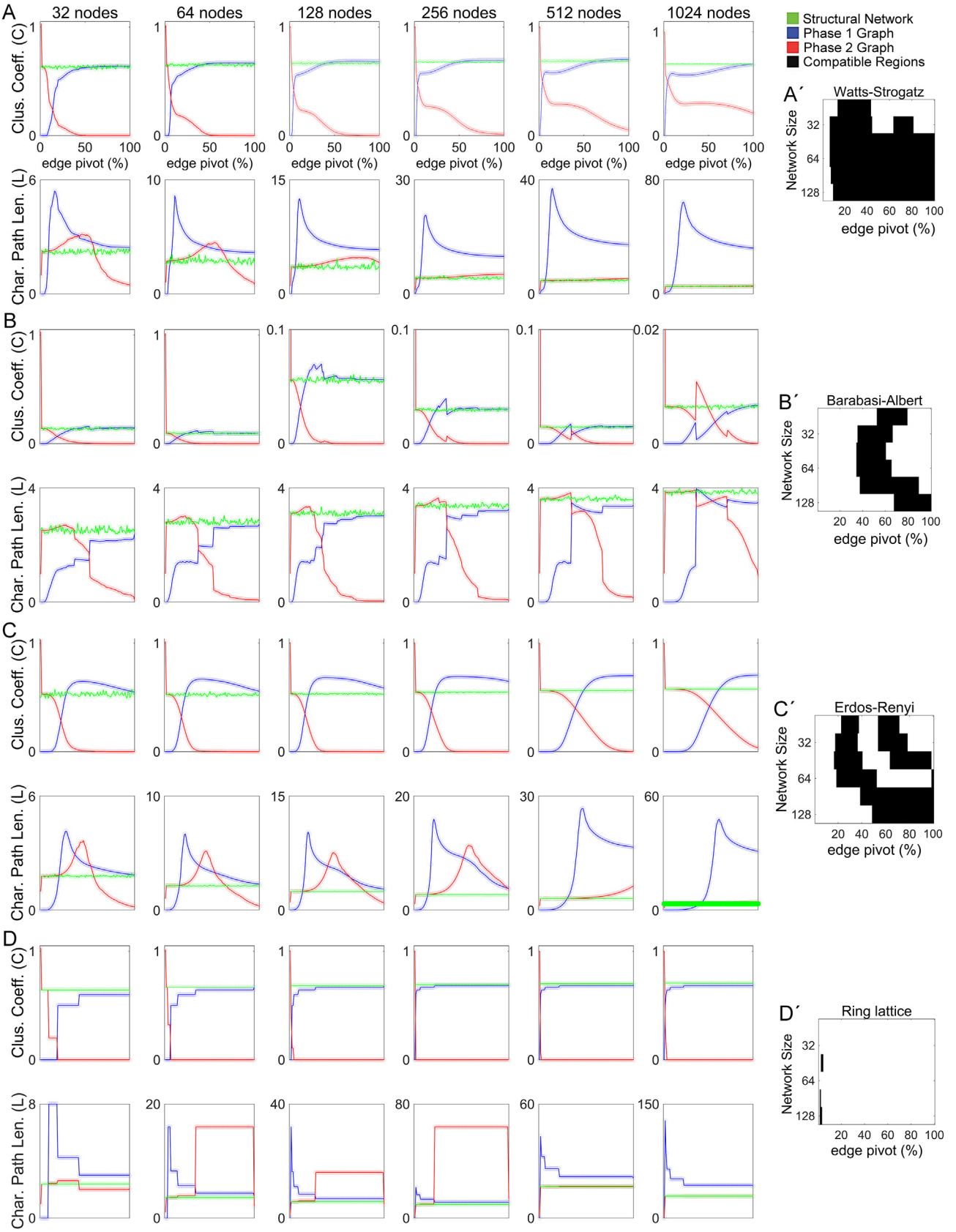

Fig. 5. Network statistics of the network models for sizes ranging from 32 to 1024 in dyadic scales. Analyzed models were: the Watts–Strogatz (A), the Barabasi–Albert (B), the Erdős–Renyi (C) and the ring lattice (D). The first row of each subfigure indicates the Clustering Coefficient while the second one the Characteristic Path Length. Besides, subfigures A′–D′ represent the related admissible regions respectively computed for each model. More plausible models are the Watts–Strogatz and the Barabasi–Albert even though the Erdős–Renyi shows a good consistence with our hypothesis despite its much lower plausibility as brain topology.

Please cite this article in press as: Zippo AG et al. Alternating Dynamics of Segregation and Integration in Human EEG Functional Networks During Working-memory Task. Neuroscience (2017), https://doi.org/10.1016/j.neuroscience.2017.12.004

Segregation may constitute the groundings of the first stages of cognitive processing in 2-back trials when (1) a greater quantity of information needs to be held on-line in order to effectively fulfill the task goals and (2) potential sources of noise (i.e. internal or external) need to be hindered to avoid interference with task-relevant information, thus setting the premises for functional integration between salient processing elements. Furthermore, a 2-back trial taxes cognitive processing in terms of WM load to a higher degree, which seems to translate in an increase in segregation but also modular consistency across participants in WM processes (Pessoa et al., 2002). Modularity is a distinctive property of a complex and efficient biological system, which tends to establish only sparse connections between sub-networks in order to scale down the propagation of noise in the system granting integration of information for demanding tasks.

According to our results, WM can be theorized as a modular system requiring high levels of segregation in the first stages of cognitive processing both to maintain salient information no longer available and to halt interference from internal or external noise generated by competing targets. Segregation is then followed by integration in order to share and efficaciously tailor information to the specific task objectives. Wrong trials, where participants failed to get correct answers, showed very divergent network dynamics. Our synthetic network models built with the nomological scaffold as from natural data supported the prospected theory. Essentially, our results suggest that brain networks observed in the functional substrates emerge as recurrent dynamics figures virtually observable at diverse spatial and temporal scales in agreement with the findings that many brain physiology episodes are scale-free (Ekman et al., 2012). The faulty "integration-segregation" scheme in wrong trials might lead to wonder how much many brain diseases associated to cognitive impairments could harbor interfering mechanisms or exhibit weakened local dynamics to generate sound state cycling. This would also suggest that functional networks might also represent a powerful tool to discriminate normal conditions from a large repertoire of diseases.

This suggestive two-step figure doesn't appear a standout in the physiology of living systems offering many examples of binary discrete phases such as diastoles and systoles for the hearth, air inhalations and exhalations for the lung, relaxations and contractions for the gastrointestinal peristalsis, etc. Hence, segregations and integrations for brain functional networks should not appear a remote concept nor an exceedingly reductive mechanism yet compared with the huge repertoire of states expressible by the human brain.

Theoretical significance

From the last section we concluded that network models, where nodes have a heavy-tailed distribution, were potentially consistent with our empirical observations from EEG activity. We further propose that these centrality distributions suggest a hierarchical processing likely divided in three layers.

A part of the experimental results showed invariances of global centralities within task trials, an important factor in the present study (Figs. 6 and 7). By taking into account that the BC in the synthetic network models used in the previous section have a similar heavy-tailed shape (Fig. 8A, except for RL) of those observed in EEG functional networks (Fig. 8B, for a wide range of binarization thresholds), we assumed that BC could predict the network node roles thus representing a sort of estimator of the structural-to-functional network mapping (Goh et al., 2001; Ekman et al., 2012; Vlachos et al., 2012; Kumar et al., 2013; Zippo et al., 2013a,b).

Accordingly, we propose an accompanying toy network model, where nodes with low BC represent the periphery of the network and nodes with highest BC represent the core of the network, arguing that these classifications could capture the essence of the alternating phenomenon. Specifically, the toy network has a 3-layer hierarchical layout by partitioning the BC values in three arbitrary classes suggested by the BC distribution shape (see Fig. 8C), with edges oriented from periphery to core (Fig. 8D, E). In the ideal information flow within the toy network, a relevant part of the peripheral nodes (in layer I) are activated, then triggering a sparse activation of other layer I nodes and of a downsized number of layer II nodes. Subsequently, activated layer II nodes similarly provoke activations of layer III nodes. Collectively, the hierarchical dynamics might be inherently reduced to two stages: activations from layer I to layer II and activations from layer II to layer III (see Fig. 8F, G). In this toy network, the functional connectivity graph of each stage is acquired by inspection of the activated edges in the current stage (violet edges in Fig. 8F, G). Intuitively, in the first stage the functional segregation strongly prevails on functional integration because modules activate their inner connections but remain mutually isolated (Fig. 8F). Conversely, in the second stage, the functional integration dominates because, although fewer modules are active (being now first layer modules, the most conspicuous, inactive), they have gone tightly connected together.

Simulation interpretations

Several synthetic network models could produce the functional dynamics observed in our experiments. The simulation endorsed the possibility that the mechanisms observed in EEG sessions are due to the inherent topological brain organization which displays specialized modules able to convey processed information in fast communicating central modules of interconnected hubs. Simulated networks preferred an edge-centric perspective of the network dynamics because classical studies of neuronal network dynamics which use node behaviors (e.g. integrate and fire, Izhikevich, Hodgkin–Huxley models) are dramatically affected by the choice of model and parameters.

Although we hypothesized and verified that small-world and core-periphery networks were consistent with experimental data, we unexpectedly found that also random networks could support the observed

Please cite this article in press as: Zippo AG et al. Alternating Dynamics of Segregation and Integration in Human EEG Functional Networks During Working-memory Task. Neuroscience (2017), https://doi.org/10.1016/j.neuroscience.2017.12.004

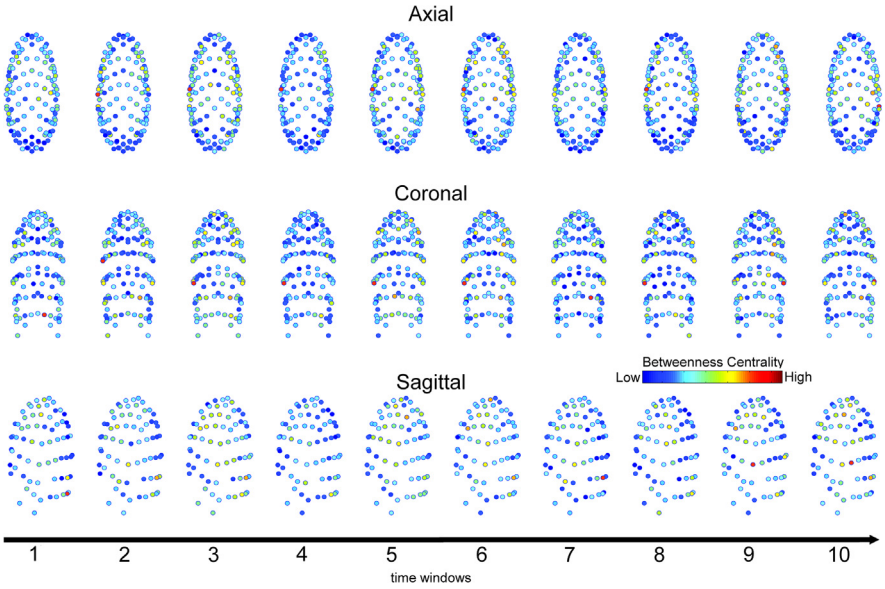

Fig. 6. Betweenness centrality distribution over the EEG electrodes. Instance of the 2-back trial depicted in the BESA sphere space where nodes correspond to the EEG electrodes (128) and numbers (1–10) correspond to the time windows. Values are averaged on all trials and subjects. Node sizes are constant and node colors indicate the level of betweenness centrality.

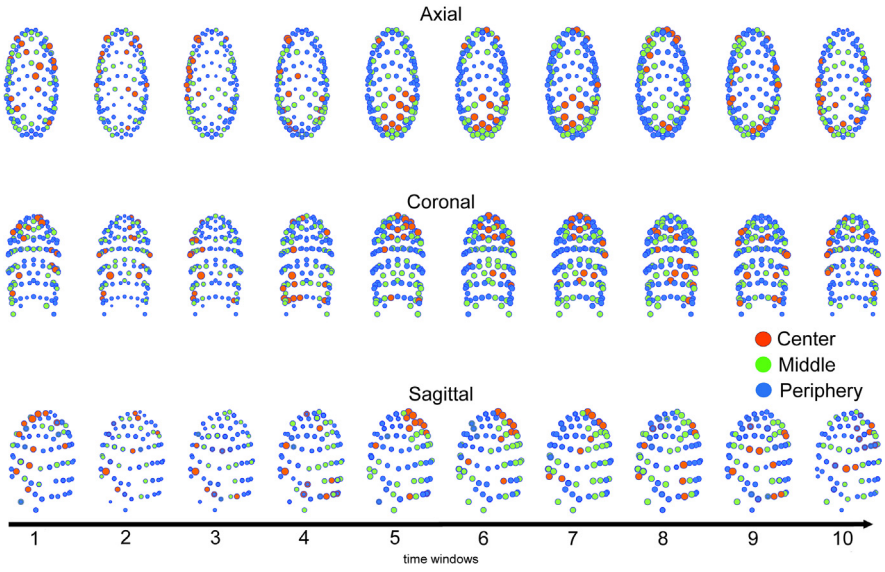

Fig. 7. Instance of the 2-back trial depicted in the BESA sphere space where nodes correspond to the EEG electrodes (128) and numbers (1–10) correspond to the time windows. Node diameters are proportional to the node degree distribution and node colors indicate the level of betweenness centrality (low → network periphery, high → middle, extremely high → network center). To note that smaller nodes mean smaller node degree and, since they were tightly correlated, smaller L. In particular, the figure shows how networks evolved during a representative single trial where the node size is proportional to the node degree and the node color is referred to the BC class (red for the class (iii), green for the class (ii) and blue for the class (i)). The windows 2, 3 and 4 highlight core activations (with nodes that switch to red and become larger) of the parietal electrodes likely recording the dorsal stream activity emergent during visual guided tasks [1,2]. This appears to represent the phase of functional segregation dominance. Subsequently, they become progressively smaller and smaller in the next windows 5, 6, 7 as potential sign of the incoming integrative processes. (Above) Axial view, (Middle) Coronal view, (Below) Sagittal view. (For interpretation of the references to color in this figure legend, the reader is referred to the web version of this article.)

topological phenomena. Indeed, although brain networks are far from being random, random networks have a heavy-tailed distribution of the node (or edge) centrality and we identified this property as the main cause for the detected topological phenomenon.

The *gedanken experiment* further suggested that the observed 2-step frame could be the result of a stable hierarchical information processing layout, organized in three layers, periphery, median and core nodes, in networks with a modules-and-hubs organization. Such an organization suggests a specific computational workflow where parallel computations in segregated modules (with low centrality) spread activity to the second layer of the hierarchy (segregation stage). The activated second layer nodes (hubs) inject the obtained computed information into the last most central nodes, which reside in the third hierarchy layer (integration stage). Although the hierarchical layout in our network model based on the node centrality was postulated, the brain hierarchical organization and the hierarchical information processing in neural circuits have been largely reported. Although the bottom-up hierarchical layout in our network model based on the node centrality was postulated, the brain hierarchical organization and the hierarchical information processing in neural circuits have been largely reported (Riesenhuber and Poggio, 1999; Meunier et al., 2010; Zippo et al., 2013a,b).

Limitations and conclusions

A note has to be spent on earlier events that may generate, modulate or influence the double step of segregation and integration in these memory tasks. Precocious signs of segregation are detectable at 300 ms from the start of the task and flourish throughout the time window up to 700 ms. Timings appear consistently overlapping with P300 waves, at least with later component of P300, the so called the P3b associated to information processing

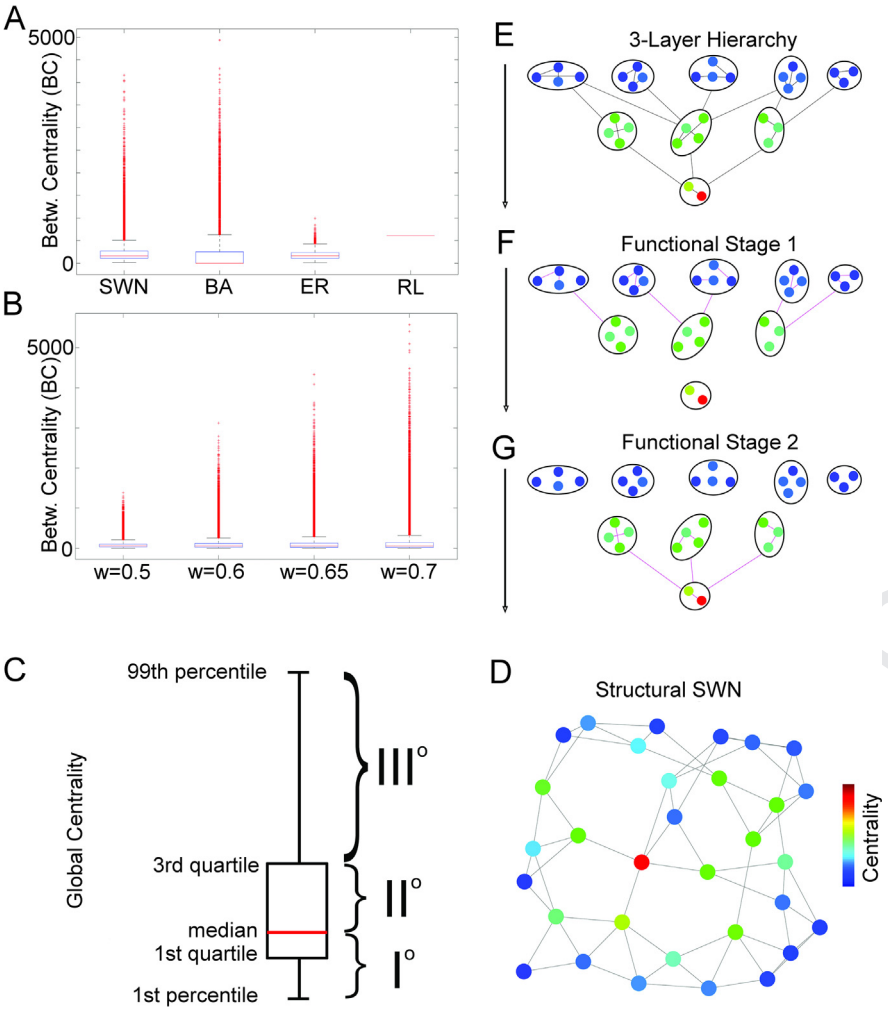

Fig. 8. (A) Comparisons between the betweenness centrality (BC) computed on the considered network models, namely the Watts–Strogatz (SWN), the Barabasi–Albert (BA), the Erdős–Renyi (ER) and the ring lattice (RL). The SWN, BA and ER showed and heavy-tailed distribution of BC similar to those computed in EEG graphs with different thresholds. (C) The heavy-tailed shape of betweenness centrality can be reasonably parted in the classes: (I) values from first to fiftieth percentiles; (II) values from fifty first percentile to third quantile; (III) values from the seventy first percentile to the ninety ninth percentile. (D) The betweenness centrality distribution on the node of a small-world network. Blue denotes nodes with low centrality, red denotes nodes with high centrality. (E) Nodes with low levels of centrality lay on the first layer of the hierarchy (different blue shades), nodes with high levels of centrality lay on the second layer of hierarchy (different green shades) and nodes with highest levels of centrality lay on the third layer (yellow and red). (F) A hypothetical stimulation of a first layer node portion activates edges (the functional connections, displayed in violet) and is named Functional Stage 1. (G) In the subsequent time step, the Functional Stage 2, the activity spreads on the second and third layer nodes returning another set of activated edges. (For interpretation of the references to color in this figure legend, the reader is referred to the web version of this article.)

(Squires et al., 1975). How much these multifarious components may contribute to the complex and late events of segregation and integration remains to be elucidated. As well, it remains unanswered which potential roles that precursor episodes of task error detection such as the error related negativity (Ne or ERN) and positivity (Pe), a couple of error monitoring processes, may have in interfering with the ensuing correct development of high cognitive-related processing of memorization (Falkenstein et al., 1991; Gehring et al., 1993). In the presence of Ne and Pe there could be generated destructive conditions leading to the abortion of the memorization processing. This is particularly important when considering that late P300 (a cognitive decisional ERP label) and Pe waves may represent a complex but partially overlapped neural processing with only slight temporal shifts (where Pe is present). In summary, it still remains to be clarified if in the presence of early errors, such as an incorrect motor planning, this may then drive a downstream deconstruction of the complex duet of segregation-integration and its behavioral counterpart related to memorization. Eventually, further studies are necessary to investigate the relations with the brain structural substrate. Unfortunately, no anatomical inference was possible with the available experimental setup.

In conclusion, the results in this study support the idea that, facing space–time limited context tasks, the human brain functional networks may work in accordance with two-step rules. Such rules could, further, be a natural consequence of the hierarchical information workflow of those networks. Therefore, the fluctuation repertories observed in brain functional networks might be elucidated by equivalent network mechanisms that would expand our comprehension of human brain network dynamics.

CONTRIBUTIONS

A.G.Z. conceived the rational of the work, designed the study, performed the experiments and analyzed the data. A. G. Z. wrote the manuscript together with G.E.M. B, P.A.D. and I. C. All of the authors made important suggestions to the manuscript and reviewed and approved the manuscript.

COMPETING INTERESTS

The authors declare no competing financial interests.

Acknowledgments—This work was partially supported by PON project 01-01297 (Virtualab). The funders had no role in study design, data collection and analysis, decision to publish, or preparation of the manuscript. The authors have declared that no competing interests exist. We wish to thank Ms. Chiara D'Aversa, Mr. Pieter Van Duin and Mr. Gian Carlo Caramenti for their helpful contributions.

REFERENCES

Allen EA, Damaraju E, Plis SM, Erhardt EB, Eichele T, Calhoun VD (2014) Tracking whole-brain connectivity dynamics in the resting state. Cereb Cortex 24:663–676.

Baddeley A (2003) Working memory: looking back and looking forward. Nat Rev Neurosci 4:829–839.

Baddeley A, Wilson BA (2002) Prose recall and amnesia: implications for the structure of working memory. Neuropsychologia 40:1737–1743.

Bassett DS, Bullmore ET, Meyer-Lindenberg A, Apud JA, Weinberger DR, Coppola R (2009) Cognitive fitness of cost-efficient brain functional networks. Proc Natl Acad Sci U S A 106:11747–11752.

Betzel RF, Erickson MA, Abell M, O'Donnell BF, Hetrick WP, Sporns O (2012) Synchronization dynamics and evidence for a repertoire of network states in resting EEG. Front Comput Neurosci 6:1–13.

Blinowska KJ, Kamiński M, Brzezicka A, Kamiński J (2013) Application of directed transfer function and network formalism for the assessment of functional connectivity in working memory task. Philos Trans R Soc London A Math Phys Eng Sci 371:20110614.

Borgatti SP (2005) Centrality and network flow. Soc Networks 27:55–71.

Bullmore E, Sporns O (2009) Complex brain networks: graph theoretical analysis of structural and functional systems. Nat Rev Neurosci 10:186–198.

Bullmore E, Sporns O (2012) The economy of brain network organization. Nat Rev Neurosci 13:336–349.

Chu CJ, Kramer MA, Pathmanathan J, Bianchi MT, Westover MB, Wizon L, Cash SS (2012) Emergence of stable functional networks in long-term human electroencephalography. J Neurosci 32:2703–2713.

Crossley NA, Mechelli A, Vértes PE, Winton-Brown TT, Patel AX, Ginestet CE, McGuire P, Bullmore ET (2013) Cognitive relevance of the community structure of the human brain functional coactivation network. Proc Natl Acad Sci U S A 110:11583–11588.

Delorme A, Makeig S (2004) EEGLAB: an open source toolbox for analysis of single-trial EEG dynamics including independent component analysis. J Neurosci Methods 134:9–21.

Dimitriadis SI, Salis C, Tarnanas I, Linden DE (2017) Topological filtering of dynamic functional brain networks unfolds informative chronnectomics: a novel data-driven thresholding scheme based on orthogonal minimal spanning trees (OMSTs). Front Neuroinform 11:28.

Ekman M, Derrfuss J, Tittgemeyer M, Fiebach CJ (2012) Predicting errors from reconfiguration patterns in human brain networks. Proc Natl Acad Sci USA 109:16714–16719.

Falkenstein M, Hohnsbein J, Hoormann J, Blanke L (1991) Effects of crossmodal divided attention on late ERP components. II. Error processing in choice reaction tasks. Electroencephalogr Clin Neurophysiol 78:447–455.

Freeman LC (1977) A set of measures of centrality based on betweenness. Sociometry 40:35–41.

Gehring WJ, Goss B, Coles MGH, Meyer DE, Donchin E (1993) A neural system for error detection and compensation. Psychol Sci 4:385–390.

Goh KI, Kahng B, Kim D (2001) Universal behavior of load distribution in scale-free networks. Phys Rev Lett 87:278701.

Gordon SM, Franaszczuk PJ, Hairston WD, Vindiola M, McDowell K (2013) Comparing parametric and nonparametric methods for detecting phase synchronization in EEG. J Neurosci Methods 212:247–258.

Gould PR (2016) On the Geographical Interpretation of Eigenvalues. 44:15–41.

Grady D, Thiemann C, Brockmann D (2012) Robust classification of salient links in complex networks. Nat Commun 3:864.

Hutchison RM, Womelsdorf T, Allen EA, Bandettini PA, Calhoun VD, Corbetta M, Della Penna S, Duyn JH, Glover GH, Gonzalez-Castillo J, Handwerker DA, Keilholz S, Kiviniemi V, Leopold DA, de Pasquale F, Sporns O, Walter M, Chang C (2013a) Dynamic functional connectivity: promise, issues, and interpretations. Neuroimage 80:360–378.

Hutchison RM, Womelsdorf T, Gati JS, Everling S, Menon RS (2013b) Resting-state networks show dynamic functional connectivity in awake humans and anesthetized macaques. Hum Brain Mapp 34:2154–2177.

Jaeggi SM, Seewer R, Nirkko AC, Eckstein D, Schroth G, Groner R, Gutbrod K (2003) Does excessive memory load attenuate activation in the prefrontal cortex? Load-dependent processing in single and dual tasks: functional magnetic resonance imaging study. Neuroimage 19:210–225.

Kitzbichler MG, Henson RN, Smith ML A, Nathan PJ, Bullmore ET (2011) Cognitive effort drives workspace configuration of human brain functional networks. J Neurosci 31:8259–8270.

Kumar A, Vlachos I, Aertsen A, Boucsein C (2013) Challenges of understanding brain function by selective modulation of neuronal subpopulations. Trends Neurosci 36:579–589.

Lefebvre E, Blondel Vincent D, Guillaume Jean-Loup, Lambiotte R (2008) Fast unfolding of communities in large networks. J Stat Mech Theory Exp 2008:P10008.

Meunier D, Lambiotte R, Bullmore ET (2010) Modular and hierarchically modular organization of brain networks. Front Neurosci 4:200.

Newman MEJ (2006) Modularity and community structure in networks. Proc Natl Acad Sci U S A 103:8577–8582.

Oberauer K (2003) Selective attention to elements in working memory. Exp Psychol 50:257–269.

Oberauer K, Suss HM (2000) Working memory and interference: a comment on Jenkins, Myerson, Hale, and Fry (1999). Psychon Bull Rev 7:727–740.

Ortiz E, Stingl K, Munssinger J, Braun C, Preissl H, Belardinelli P (2012) Weighted phase lag index and graph analysis: preliminary investigation of functional connectivity during resting state in children. Comput Math Methods Med 2012:186353.

Owen AM, McMillan KM, Laird AR, Bullmore E (2005) N-back working memory paradigm: a meta-analysis of normative functional neuroimaging studies. Hum Brain Mapp 25:46–59.

Palva JM, Zhigalov A, Hirvonen J, Korhonen O, Linkenkaer-Hansen K, Palva S (2013) Neuronal long-range temporal correlations and avalanche dynamics are correlated with behavioral scaling laws. Proc Natl Acad Sci U S A 110:3585–3590.

Park H-J, Friston K (2013) Structural and functional brain networks: from connections to cognition. Science 342:1238411.

Pessoa L, Gutierrez E, Bandettini P, Ungerleider L (2002) Neural correlates of visual working memory: fMRI amplitude predicts task performance. Neuron 35:975–987.

Riesenhuber M, Poggio T (1999) Hierarchical models of object recognition in cortex. Nat Neurosci 2:1019–1025.

Rubinov M, Sporns O (2010) Complex network measures of brain connectivity: uses and interpretations. Neuroimage 52:1059–1069.

Rubinov M, Sporns O (2011) Weight-conserving characterization of complex functional brain networks. Neuroimage 56:2068–2079.

Senden M, Deco G, De Reus MA, Goebel R, Van Den Heuvel MP (2014) Rich club organization supports a diverse set of functional network configurations. Neuroimage 96:174–182.

Sporns O (2013a) Network attributes for segregation and integration in the human brain. Curr Opin Neurobiol 23:162–171.

Sporns O (2013b) Making sense of brain network data. Nat Methods 10:491–493.

Squires NK, Squires KC, Hillyard SA (1975) Two varieties of long-latency positive waves evoked by unpredictable auditory stimuli in man. Electroencephalogr Clin Neurophysiol 38:387–401.

Tononi G, Edelman GM, Sporns O (1998) Complexity and coherency: integrating information in the brain. Trends Cogn Sci 2:474–484.

Tononi G, Sporns O, Edelman GM (1994) A measure for brain complexity: relating functional segregation and integration in the nervous system. Proc Natl Acad Sci U S A 91:5033–5037.

Van de Ville D, Britz J, Michel CM (2010) EEG microstate sequences in healthy humans at rest reveal scale-free dynamics. Proc Natl Acad Sci U S A 107:18179–18184.

Please cite this article in press as: Zippo AG et al. Alternating Dynamics of Segregation and Integration in Human EEG Functional Networks During Working-memory Task. Neuroscience (2017), https://doi.org/10.1016/j.neuroscience.2017.12.004

van den Heuvel MP, Sporns O (2011) Rich-club organization of the human connectome. J Neurosci 31:15775–15786.
van den Heuvel MP, Stam CJ, Boersma M, Hulshoff Pol HE (2008) Small-world and scale-free organization of voxel-based resting-state functional connectivity in the human brain. Neuroimage 43:528–539.
Vinck M, Oostenveld R, van Wingerden M, Battaglia F, Pennartz CMA (2011) An improved index of phase-synchronization for electrophysiological data in the presence of volume-conduction, noise and sample-size bias. Neuroimage 55:1548–1565.
Vlachos I, Aertsen A, Kumar A (2012) Beyond statistical significance: implications of network structure on neuronal activity. PLoS Comput Biol 8:e1002311.
Watts DJ, Strogatz SH (1998) Collective dynamics of ''small-world'' networks. Nature 393:440–442.
Whitlow CT, Casanova R, Maldjian JA (2011) Effect of Resting-State Functional MR Imaging Duration on Stability of Graph Theory Metrics of Brain Network Methods: Results, 259.
Zippo AG, Gelsomino G, Van Duin P, Nencini S, Caramenti GC, Valente M, Biella GEM (2013a) Small-world networks in neuronal populations: a computational perspective. Neural Netw 44:143–156.
Zippo AG, Storchi R, Nencini S, Caramenti GC, Valente M, Biella GEM (2013b) Neuronal functional connection graphs among multiple areas of the rat somatosensory system during spontaneous and evoked activities Sporns O, ed. PLoS Comput Biol 9:e1003104.

APPENDIX A

Appendix. The complex network statistics used in this work. We reported the weighted versions of each statistic. Weights w are assumed to span from 0 to 1.

Measure	Definition	Interpretation
Node strength	$k_i = \sum_{j \in N} w_{ij}$	Sum of the edge weights of a given node i. Nodes with relatively high values of k are called *hubs*
Shortest weighted path length	$d_{ij} = \sum_{w_{fg} \in r_{i \leftrightarrow j}} 1/w_{fg}$ where $r_{i \leftrightarrow j}$ is the shortest weighted path between i and j	The sum of the inverse of edge weights encountered in the shortest path between node i and j
Characteristic path length	$L = \frac{1}{n}\sum_{i \in N} L_i = \frac{1}{n}\sum_{i \in N} \frac{\sum_{j \in N, j \neq i} d_{ij}}{n-1}$	Measure of network integration
Clustering coefficient	$C = \frac{1}{n}\sum_{i \in N} C_i = \frac{1}{n}\sum_{i \in N} \frac{2t_i}{k_i(k_i-1)}$, with $t_i = \frac{1}{2}\sum_{j,h \in N} (aw_{ij} aw_{ih} aw_{jh})^{1/3}$	Measure of fine-grain network segregation. It counts the average number of triangles t (3-node fully connected graphs) present in the network
Modularity	$Q = \frac{1}{l}\sum_{u,v \in N} [w_{uv} - \frac{\Omega_i \Omega_j}{l}] \delta_{m_i} \delta_{m_j}$, where l is the sum of all weights of V (whose elements are called *modules*) and m_i is the module containing the node i and $\delta_{m_i}\delta_{m_j} = 1$ if $m_i = m_j$ and 0 otherwise.	It evaluates the tendency of the network to be reduced in independent (or scarcely dependent) modules
Eigenvector centrality	$EC_i = \frac{1}{\lambda}\sum_{z \in Z(v)} x_z$, where $Z(v)$ is a set of neighbors of v and λ is a constant	It assigns relative scores to nodes whose connections to high-scoring nodes contribute more to the score of the node in question than equal connections to low-scoring nodes
Betweenness centrality	$BC_i = \frac{1}{(n-1)(n-2)}\sum_{h,j \in N, h \neq j, h \neq i, i \neq j} \frac{\rho_{hj}(i)}{\rho_{hj}}$, where ρ_{hj} is the number of shortest paths between h and j, and $\rho_{hj}(i)$ is the number of shortest paths between h and j that pass through i	It is the amount of shortest paths that pass through the node i. It roughly indicates how much information burdens the node i
Small-worldness	$S = \frac{C/C^r}{L/L^r}$ $\omega = \frac{L^r}{L} - \frac{C}{C^l}$	The indices quantify the affinity of a network to be a small-world network. S should be greater than 1 and ω close to 0

(Received 18 August 2017, Accepted 4 December 2017)
(Available online xxxx)